Max-Planck-Institut für Physik

JADE Note 147
MPP-2004-100
September 6, 2004

Study of moments of event shapes in e^+e^- annihilation using JADE data

C. Pahl, S. Kluth, S. Bethke, P.A. Movilla Fernandez, J. Schieck, and the JADE Collaboration[1]

Abstract

Data from e^+e^- annihilation into hadrons collected by the JADE experiment at centre-of-mass energies between 14 GeV and 44 GeV were used to study moments of event shape distributions. The data were compared with Monte Carlo models and with predictions from QCD NLO order calculations. The strong coupling constant measured from the moments is

$$\alpha_S(M_{Z^0}) = 0.1286 \pm 0.0007(\text{stat.}) \pm 0.0011(\text{exp.}) \pm 0.0022(\text{had.}) \pm 0.0068(\text{theo.}),$$
$$\alpha_S(M_{Z^0}) = 0.1286 \pm 0.0072 \text{ (total error)}$$

consistent with the world average. However, systematic deficiencies in the QCD NLO order predictions are visible for some of the higher moments.

This note describes preliminary JADE results

[1] See [1] for the full list of authors

1 Introduction

The annihilation of an electron and a positron into hadrons allows precise tests of Quantum Chromodynamics (QCD). Commonly jet production rates or distributions of event shape observables have been studied. Predictions by perturbative QCD combined with hadronization corrections derived from models have been found to describe the data at low and high energies well, see e.g. [2–4].

In this analysis we used data collected by the JADE experiment in the years 1979 to 1986 at the PETRA e^+e^- collider at DESY at six centre-of-mass energies $\sqrt{s}$ covering the range of 14–44 GeV. We measured the first five moments of event shape observables for the first time in this $\sqrt{s}$ region in e^+e^- annihilation and compared the data to predictions by Monte Carlo Models and by perturbative QCD. From the comparison of the data with the theory we extracted the strong coupling constant α_S.

The outline of the note is as follows. In section 2, we define the observables used in the analysis and describe the perturbative QCD predictions. In section 3 the analysis procedure is explained in detail. Section 4 contains the discussion of the systematic checks which were performed and the resulting systematic errors. We collect our results in section 5 and summarize them in section 6.

2 Observables

The properties of hadronic events may be characterized by a set of event shape observables. These may be used to characterize the distribution of particles and thus the topology of an event as "pencil-like", planar, spherical etc. They can be computed either using the measured charged particle tracks and calorimeter clusters, or using the true hadrons or partons in simulated events. The following event shapes were considered here:

Thrust T: defined by the expression [5, 6]

$$T = \max_{\vec{n}} \left(\frac{\sum_i |\vec{p}_i \cdot \vec{n}|}{\sum_i |p_i|} \right) \quad .$$

The thrust axis $\vec{n}_T$ is the direction $\vec{n}$ which maximizes the expression in parentheses. A plane through the origin and perpendicular to $\vec{n}_T$ divides the event into two hemispheres H_1 and H_2.

***C*-parameter:** The linearized momentum tensor $\Theta^{\alpha\beta}$ is defined by

$$\Theta^{\alpha\beta} = \frac{\sum_i (p_i^\alpha p_i^\beta)/|\vec{p}_i|}{\sum_i |\vec{p}_i|} \quad , \quad \alpha, \beta = 1, 2, 3 \quad .$$

The three eigenvalues λ_j of this tensor define C [7] through

$$C = 3(\lambda_1\lambda_2 + \lambda_2\lambda_3 + \lambda_3\lambda_1) \quad .$$

Heavy Jet Mass M_H: The hemisphere invariant masses are calculated using the particles in the two hemispheres H_1 and H_2. We define M_H [8, 9] as the heavier mass, divided by $\sqrt{s}$.

Jet Broadening observables B_T and B_W: These are defined by computing the quantity

$$B_k = \left(\frac{\sum_{i \in H_k} |\vec{p}_i \times \vec{n}_T|}{2 \sum_i |\vec{p}_i|} \right)$$

for each of the two event hemispheres, H_k, defined above. The two observables [10] are defined by

$$B_T = B_1 + B_2 \ , \quad \text{and} \quad B_W = \max(B_1, B_2)$$

where B_T is the total and B_W is the wide jet broadening.

Transition value between 2 and 3 jets y_{23}: Jet algorithms are applied to cluster the large number of particles of an hadronic event into a small number of jets, reflecting the parton structure of the event. For this analysis we used the Durham scheme [11]. Defining each particle initially to be a jet, a resolution variable y_{ij} is calculated for each pair of jets i and j:

$$y_{ij} = \frac{2\min(E_i^2, E_j^2)}{E_{\text{vis}}^2}(1 - \cos\theta_{ij}), \tag{1}$$

where E_i and E_j are the energies, $\cos\theta_{ij}$ is the angle between the two jets and E_{vis} is the sum of the energies of all visible particles in the event (or the partons in a theoretical calculation). If the smallest value of y_{ij} is less than a predefined value y_{cut}, the pair is replaced by a jet with four momentum $p_{ij}^\mu = p_i^\mu + p_j^\mu$, and the clustering starts again with p_{ij}^μ instead of the momenta p_i^μ and p_j^μ. Clustering ends when the smallest value of y_{ij} is larger than y_{cut}. The remaining jets are then counted. The value of y_{cut} at which for an event the transition between a 2-jet and a 3-jet assignment occurs is called y_{23}.

In the following discussion, whenever we wish to refer to a generic event shape observable we use the symbol y. In almost all cases, larger values of y indicate regions dominated by the radiation of hard gluons and small values of y indicate the region influenced by multiple soft gluon radiation. Note that thrust T forms an exception to this rule, as the value of T reaches unity for events consisting of two collimated back-to-back jets. We therefore use $y = 1 - T$ instead. For all of these event shapes, a perfectly collimated ("pencil-like") two-jet final state will have $y = 0$.

The nth, $n = 1, 2, \ldots$, moment of the distribution of an event shape observable y is defined by

$$\langle y^n \rangle = \int_0^{y_{max}} y^n \frac{1}{\sigma} \frac{\mathrm{d}\sigma}{\mathrm{d}y} \mathrm{d}y \quad ,$$

where y_{max} is the kinematically allowed upper limit of the observable. The calculations always involve a full integration over phase space, which implies that comparison with data always probes all of the available phase space. This is in contrast to QCD predictions for distributions; these are commonly only compared with data, e.g. in order to measure α_S, in restricted regions, where the theory is able to describe the data well, see e.g. [2]. Comparisons of QCD predictions for moments of event shape distributions with data are thus complementary to tests of the theory using the differential distributions.

The formula for the $\mathcal{O}(\alpha_S^2)$ QCD prediction of $\langle y^n \rangle$ is with $\bar{\alpha}_S = \alpha_S/(2\pi)$

$$\langle y^n \rangle = \mathcal{A}_n \bar{\alpha}_S + \mathcal{B}_n \bar{\alpha}_S^2 \tag{2}$$

involving the $\mathcal{O}(\alpha_S)$ coefficients $\mathcal{A}_n$ and $\mathcal{O}(\alpha_S^2)$ coefficients $\mathcal{B}_n$. The values of the coefficients $\mathcal{A}_n$ and $\mathcal{B}_n$ can be obtained by numerical integration of the QCD matrix elements using the program EVENT2 [12].

The QCD prediction depends on the renormalization scale μ, see e.g. [13]. The renormalization scale factor is defined as $x_\mu = \mu/\sqrt{s}$ implying that $\bar{\alpha}_S = \bar{\alpha}_S(\mu)$ in equ. (2). A truncated fixed order QCD calculation such as equ. (2) will depend on x_μ. The renormalization scale dependence is implemented by the replacement $\mathcal{B}_n \to \mathcal{B}_n + \beta_0 \ln x_\mu \mathcal{A}_n$ where $\beta_0 = 11 - \frac{2}{3} n_f$ is the leading order β-function coefficient of the renormalization group equation and $n_f = 5$ is the number of active quark flavours.

The data are normalized to the total hadronic cross section $\sigma_{tot} = \sigma_0(1 + \alpha_S/\pi)$ in LO while the QCD calculations are normalized to the born cross section σ_0. Thus a correction has to be applied by making the replacement $\mathcal{B}_n \to \mathcal{B}_n - 2\mathcal{A}_n$.

3 Analysis Procedure

3.1 The JADE Detector

A detailed description of the JADE detector can be found in [1]. This analysis relies mainly on the reconstruction of charged particle trajectories and on the measurement of energy deposited in the electromagnetic calorimeter. Tracking of charged particles was performed with the central detector, which was positioned in a solenoidal magnet providing an axial magnetic field of 0.48 T. The central detector contained a large volume jet chamber. Later a vertex chamber close to the interaction point and surrounding z-chambers to measure the z-coordinate [2] were added. Most of the tracking information was obtained from the jet chamber, which provided up to 48 measured space points per track, and good tracking efficiency in the region $|\cos\theta| < 0.97$. Electromagnetic energy was measured by the lead glass calorimeter surrounding the magnet coil, separated into a barrel ($|\cos\theta| < 0.839$) and two end-cap ($0.86 < |\cos\theta| < 0.97$) sections. The electromagnetic calorimeter consisted of 2520 lead glass blocks with a depth of 12.5 radiation lengths in the barrel (since 1983 increased to 15.7 in the middle 20% of the barrel) and 192 lead glass blocks with 9.6 radiation lengths in the end-caps.

3.2 Data Samples

The data used in this analysis were collected by JADE between 1979 and 1986 and correspond to a total integrated luminosity of 195 pb^{-1}. The breakdown of the data samples, mean centre-of-mass energy, energy range, data taking period, collected integrated luminosities and the size of the data samples after selection of hadronic events are given in

[2] In the JADE right-handed coordinate system the $+x$ axis pointed towards the centre of the PETRA ring, the y axis pointed upwards and the z axis pointed in the direction of the electron beam. The polar angle θ and the azimuthal angle ϕ were defined with respect to z and x, respectively, while r was the distance from the z-axis.

table 1. The data samples were chosen following previous analyses, e.g. [1–4, 14]. The data are available from two versions of the reconstruction software from 9/87 and from 5/88. We used both sets and considered differences between the results as an experimental systematic uncertainty.

average energy in GeV	energy range in GeV	year	luminosity (pb^{-1})	selected events 9/87	selected events 5/88
14.0	13.0–15.0	1981	1.46	1722	1783
22.0	21.0–23.0	1981	2.41	1383	1403
34.6	33.8–36.0	1981–1982	61.7	14213	14313
35.0	34.0–36.0	1986	92.3	20647	20876
38.3	37.3–39.3	1985	8.28	1584	1585
43.8	43.4–46.4	1984–1985	28.8	3896	4376

Table 1: The average center-of-mass energy, energy range, year of data taking and integrated luminosity for each data sample, together with the numbers of selected data events using the data sample version of 9/87 or 5/88.

3.3 Monte Carlo Samples

Samples of Monte Carlo simulated events were used to correct the data for experimental acceptance and backgrounds. The process $e^+e^- \rightarrow$ hadrons was simulated using PYTHIA 5.7 [15]. Corresponding samples using HERWIG 5.9 [16, 17] were used for systematic checks. The Monte Carlo samples generated at each energy point were processed through a full simulation of the JADE detector [18–20], summarized in [14], and reconstructed in essentially the same way as the data.

In addition, for comparisons with the corrected data, and when correcting for the effects of fragmentation, large samples of Monte Carlo events without detector simulation were employed, using the parton shower models PYTHIA 6.158, HERWIG 6.2 and ARIADNE 4.11 [21]. All models were adjusted to LEP 1 data by the OPAL collaboration.

The ARIADNE Monte Carlo generator is based on a color dipole mechanism for the parton shower. The PYTHIA and HERWIG Monte Carlo programs use the leading logarithmic approximation (LLA) approach to model the emission of gluons in the parton shower. For the emission of the first hard gluon, the differences between the LLA approach and a leading order matrix element calculation are accounted for. However, the emission of gluons later on in the parton shower is based only on a LLA cascade and is expected to differ from a complete matrix element calculation. For this reason we do expect deviations in the description of the data by the Monte Carlo models. Recently new Monte Carlo generators have been developed, which implement a more complete simulation of the hard parton emission [22]. However, the models are not yet tuned to data taken at LEP and were therefore not considered in this analysis.

3.4 Selection of Events

The selection of events for this analysis aims to identify hadronic event candidates and to reject events with a large amount of energy emitted by initial state radiation (ISR). The selection of hadronic events was based on cuts on event multiplicity (to remove leptonic final states) and on visible energy and longitudinal momentum balance (to remove radiative and two-photon events, $e^+e^- \to e^+e^-$ hadrons). The cuts used are documented in [23–25] and summarized in a previous publication [2].

Standard criteria were used to select good tracks and clusters of energy deposits in the calorimeter for subsequent analysis. Charged particle tracks were required to have at least 20 hits in r-ϕ and at least 12 in r-z in the jet chamber. The total momentum was required to be at least 50 MeV. Furthermore, the point of closest approach of the track to the collision axis was required to be less than 5 cm from the nominal collision point in the $x-y$ plane and less than 35 cm in the $z-$direction.

In order to mitigate the effects of double counting of energy from tracks and calorimeter clusters a standard algorithm was adopted which associated charged particles with calorimeter clusters, and subtracted the estimated contribution of the charged particles from the cluster energy. Charged particle tracks were assumed to be pions while the photon hypothesis was assigned to electromagnetic energy clusters. Clusters in the electromagnetic calorimeter were required to have an energy exceeding 0.15 GeV after the subtraction of the expected energy deposit of any associated tracks. From all accepted tracks and clusters i the visible energy $E_{\rm vis} = \sum_i E_i$, momentum balance $p_{\rm bal} = |\sum_i p_{z,i}|/E_{\rm vis}$ and missing momentum $p_{\rm miss} = |\sum_i \vec{p}_i|$ were calculated. To charged particle tracks the pion mass was assigned while the mass of clusters was assumed to be zero.

Hadronic event candidates were required to pass the following selection criteria:

- The total energy deposited in the electromagnetic calorimeter had to exceed 1.2 GeV (0.2 GeV) for $\sqrt{s} < 16$ GeV, 2.0 GeV (0.4 GeV) for $16 < \sqrt{s} < 24$ GeV and 3.0 GeV (0.4 GeV) for $\sqrt{s} > 24$ GeV in the barrel (each endcap) of the detector.

- The number of good charged particle tracks was required to be greater than three reducing $\tau^+\tau^-$ and two-photon backgrounds to a negligible level.

- For events with exactly four tracks configurations with three tracks in one hemisphere and one track in the opposite hemisphere were rejected.

- At least three tracks had to have more than 24 hits in $r-\phi$ and a momentum larger than 500 MeV; these tracks are called long tracks.

- The visible energy had to fulfill $E_{\rm vis}/\sqrt{s} > 0.5$.

- The momentum balance had to fulfill $p_{\rm bal} < 0.4$.

- The missing momentum had to fulfill $p_{\rm miss}/\sqrt{s} < 0.3$.

- The z-coordinate of the reconstructed event vertex had to lie within 15 cm of the interaction point.

- The polar angle of the thrust axis was required to satisfy $|\cos(\theta_{\mathrm{T}})| < 0.8$ in order that the events be well contained in the detector acceptance.

The numbers of selected events for each $\sqrt{s}$ are shown in table 1 for the two versions of the data.

3.5 Corrections to the Data

All selected tracks and the electromagnetic calorimeter clusters remaining after correcting for double counting of energy as described above were used in the evaluation of the event shape moments. The values of the moments after all selection cuts had been applied are said to be at the detector level.

In this analysis events from the process $\mathrm{e^+e^-} \to \mathrm{b\bar{b}}$ were considered as background, since especially at low $\sqrt{s}$ the large mass of the b quarks and of the subsequently produced B hadrons will influence values of the moments. The QCD predictions were calculated for massless quarks and thus we chose to correct our data for the presence of $\mathrm{b\bar{b}}$ events.

For the determination of the moments we calculated the sums $\sum_i y^n_{i,data}$ $(n = 1, \ldots, 5)$ where i denotes all selected events. The expected contribution of $\mathrm{b\bar{b}}$ background events $\sum_i y^n_{i,\mathrm{b\bar{b}}}$ was subtracted from the observed $\sum_i y^n_{i,data}$. The effects of detector acceptance and resolution and of residual ISR were then accounted for by a multiplicative correction procedure.

Two sets of $\sum_i y^n_i$ were calculated from Monte Carlo simulated signal events; the first, at the detector level, treated the Monte Carlo events identically to the data, while the second, at the hadron level, was computed using the true momenta of the stable particles in the event[3], and was restricted to events where $\sqrt{s'}$, the centre-of-mass energy reduced due to ISR, statisfied $\sqrt{s} - \sqrt{s'} < 0.15$ GeV. The Monte Carlo ratio of the hadron level to the detector level for each moment value was used as a correction factor for the data. The corrected sums were then normalized by the expected total number of events yielding the final values of $\langle y^n \rangle$. The expected total number of events was calculated from the number of selected events in the data in the same way as for the moments.

The detector correction factors C^{detector} as determined using PYTHIA and HERWIG are shown in figures 1 and 2. We observe some disagreement between the detector corrections calculated using PYTHIA or HERWIG at low $\sqrt{s}$ while at larger $\sqrt{s}$ the correction factors agree well for most observables. The difference in detector corrections was evaluated as an experimental systematic uncertainty.

4 Systematic Uncertainties

Several sources of possible systematic uncertainties were studied. All systematic uncertainties were taken as symmetric. Contributions to the experimental uncertainties were estimated by repeating the analysis with varied cuts or procedures. For each systematic variation the value of α_{S} was determined and then compared to the result of the standard analysis (default value). For each variation the difference with respect to the default value

[3] All charged and neutral particles with a lifetime larger than 3×10^{-10}s were considered stable.

was taken as a systematic uncertainty. In the cases of two-sided systematic variations the larger deviation from the default value was taken as the systematic uncertainty.

- In the standard analysis the data version from 9/87 was used. As a variation a different data set from 5/88 was used.

- In the default method the tracks and clusters were associated and the estimated energy from the tracks was subtracted. As a variation all reconstructed tracks and all electromagnetic clusters were used.

- The thrust axis was required to satisfy $|\cos(\theta_{\mathrm{T}})| < 0.7$. With this more stringent cut events were restricted to the barrel region of the detector, which provides better measurements of tracks and clusters compared to the endcaps.

- Instead of using PYTHIA for the correction of detector effects as described in section 3.5, events generated with HERWIG were used.

- The requirement on missing momentum was dropped or tightened to $p_{\mathrm{miss}}/\sqrt{s} < 0.25$.

- The requirement on the momentum balance was dropped or tightened to $p_{\mathrm{bal}} < 0.3$.

- The requirement on the number of long tracks was tightened to $N_{\mathrm{long}} \geq 4$.

- The requirement on the visible energy was varied to $E_{\mathrm{vis}}/\sqrt{s} > 0.45$ and $E_{\mathrm{vis}}/\sqrt{s} > 0.55$.

- The amount of subtracted $\mathrm{b\bar{b}}$ background was varied by $\pm 5\%$ in order to cover uncertainties in the estimation of the background fraction in the data.

All contributions listed above were added in quadrature and the result quoted as the experimental systematic uncertainty. The dominating effects were the use of the different data version followed by employing HERWIG to determine the detector corrections. In the fits of the QCD predictions to the data two further systematic uncertainties were evaluated:

- The uncertainties associated with the hadronization correction (see section 5.2) were assessed by using HERWIG and ARIADNE instead of PYTHIA. The larger change in α_{S} resulting from these alternatives was taken to define the hadronization systematic uncertainty.

- The theoretical uncertainty, associated with missing higher order terms in the theoretical prediction, was assessed by varying the renormalization scale factor x_μ. The predictions of an all-orders QCD calculation would be independent of x_μ, but a finite order calculation such as that used here retains some dependence on x_μ. The renormalization scale x_μ was set to 0.5 and 2. The larger deviation from the default value was taken as theoretical systematic uncertainty.

5 Results

5.1 Values of Event Shape Moments

The first five event shape moments for the six observables after subtraction of $b\bar{b}$ background and correction for detector effects are shown in figures 3 and 4. Superimposed we show the moments predicted by the PYTHIA, HERWIG and ARIADNE Monte Carlo models tuned by OPAL to LEP 1 data. In order to make a more clear comparison between data and models the lower plots show the differences between data and each model divided by the combined statistical and experimental error for $\sqrt{s} = 14$ and 35 GeV. The three models are seen to describe the data fairly well; PYTHIA and ARIADNE are found to agree better with the data than HERWIG.

5.2 Determination of α_S

Our measurement of the strong coupling constant α_S is based on the fits of QCD predictions to the corrected moment values, i.e. the data shown in figures 3 and 4. The theoretical predictions using the $\mathcal{O}(\alpha_S^2)$ calculation as described in section 2 provide values at the parton level. In order to confront the theory with the hadron level data, it is necessary to correct for hadronization effects. The moments were calculated at hadron and parton level using PYTHIA and, as a cross check, with the HERWIG and ARIADNE models. The data points were then multiplied by the ratio C^{had} of the parton and hadron level moment values in order to correct for hadronization.

The models use cuts on quantities like e.g. the invariant mass between partons in order to regulate divergencies in the predictions for the parton shower evolution. As a consequence in some events no parton shower is simulated and the orginal quark-antiquark pair enters the hadronization stage of the model directly. This leads to a bias in the calculation of moments at the parton level, since $y = 0$ in this case for all observables considered here. In order to avoid this bias we excluded in the simulation at the parton level events without at least one radiated gluon. At the hadron and detector level all events were used.

The hadronization correction factors C^{had} as obtained from the three models are shown in figures 5 and 6. We find that the hadronization corrections reach values of down to about 0.5 at low $\sqrt{s}$. For larger $\sqrt{s}$ the hadronization corrections decrease as expected. We also observe that the models don't agree well for moments based on B_{W}, y_{23} and M_{H} at low $\sqrt{s}$. The differences between the models were studied as a systematic uncertainty in the fits.

A χ^2-value for each moment $\langle y^n \rangle$ was calculated using the following formula:

$$\chi^2 = \sum_i (\langle y^n \rangle_i - \langle y^n \rangle_{\mathrm{theo},i})^2 / \sigma_i^2 \tag{3}$$

where i denotes the energy points. The χ^2 value was minimized with respect to $\alpha_S(M_{Z^0})$ for each moment n separately. The running of α_S was implemented in the fit in two-loop precision using the formula shown in [26]. The scale parameter x_μ, as discussed in section 2, was set to 1.

The fit results are shown in figure 7. The fit to the first moment $\langle M_{\rm H} \rangle$ did not converge and therefore no result is shown. We observe values of χ^2/d.o.f. of $\mathcal{O}(1)$; the fitted QCD predictions including the running of $\alpha_{\rm S}$ are thus consistent with our data. However, we find that for $\langle (1-T)^n \rangle$, $\langle C^n \rangle$ and $\langle B_{\rm T}^n \rangle$ the fitted values of $\alpha_{\rm S}(M_{\rm Z^0})$ increase steeply with the order n of the moment used. This effect is not as pronounced for $\langle B_{\rm W}^n \rangle$, $\langle (y_{23})^n \rangle$ and $\langle M_{\rm H}^n \rangle$, $n = 2 \ldots 5$. In order to investigate the origin of this behaviour we show in figure 8 the ratio $K = \mathcal{B}_n / \mathcal{A}_n$ of NLO and LO coefficients for the six observables used in our fits. There is a clear correlation between the steeply increasing values of $\alpha_{\rm S}(M_{\rm Z^0})$ with moment n and increasing values of K with n for $\langle (1-T)^n \rangle$, $\langle C^n \rangle$ and $\langle B_{\rm T}^n \rangle$. The other observables $\langle B_{\rm W}^n \rangle$, $\langle (y_{23})^n \rangle$ and $\langle M_{\rm H}^n \rangle$, $n = 2 \ldots 5$, have fairly constant values of K and correspondingly stable results for $\alpha_{\rm S}(M_{\rm Z^0})$. We also note that $\langle M_{\rm H} \rangle$ has a large and negative value of K which is the cause that the fit did not converge.

It is also of interest to combine the measurements of $\alpha_{\rm S}(M_{\rm Z^0})$ from the various fits in order to determine a single value. This problem has been subject of extensive study by the LEP QCD working group [27], and we adopt their procedure here.

In brief the method is as follows. The measurements of $\alpha_{\rm S}(M_{\rm Z^0})$ were combined in a weighted mean, to minimize the χ^2 between the combined value and the measurements. If the measured values of $\alpha_{\rm S}(M_{\rm Z^0})$ are denoted $\alpha_{{\rm S},i}$, with covariance matrix V', the combined value, $\alpha_{\rm S}(M_{\rm Z^0})$, is given by

$$\alpha_{\rm S}(M_{\rm Z^0}) = \sum w_i \alpha_{{\rm S},i} \quad \text{where} \quad w_i = \frac{\sum_j (V'^{-1})_{ij}}{\sum_{j,k} (V'^{-1})_{jk}}, \tag{4}$$

where i and j denote the individual results. The difficulty resides in making a reliable estimate of V' in the presence of dominant and highly correlated systematic errors. Small uncertainties in the estimation of these correlations can cause undesirable features such as negative weights. For this reason only statistical correlations and experimental systematic errors assumed to be partially correlated between measurements were taken to contribute to the off-diagonal elements of the covariance matrix: $V'_{ij} = \min(\sigma^2_{exp,i}, \sigma^2_{exp,j})$. All error contributions (statistical, experimental, hadronization and scale uncertainty) were taken to contribute to the diagonal elements. The hadronization and scale uncertainties were computed by combining the $\alpha_{\rm S}(M_{\rm Z^0})$ values obtained with the alternative hadronization models, and from setting $x_\mu = 0.5$ or $x_\mu = 2.0$, using the weights derived from the covariance matrix V'.

We considered only those results for which the NLO term in equ. (2) is less than half the LO term (i.e. $|K\alpha_{\rm S}/2\pi| < 0.5$ or $|K| < 25$), namely $\langle 1-T \rangle$, $\langle C \rangle$, $\langle B_{\rm T} \rangle$, $\langle B_{\rm W}^n \rangle$ and $\langle (y_{23})^n \rangle$, $n = 1, \ldots, 5$ and $\langle M_{\rm H}^n \rangle$, $n = 2, \ldots, 5$; i.e. results from 17 observables in total. The purpose of this requirement was to select observables with an apparently converging perturbative prediction. The K values are shown in figure 8. The statistical correlations between the 17 results were determined using Monte Carlo simulation at the hadron level.

The result of the combination is

$$\alpha_{\rm S}(M_{\rm Z^0}) = 0.1286 \pm 0.0007(\text{stat.}) \pm 0.0011(\text{exp.}) \pm 0.0022(\text{had.}) \pm 0.0068(\text{theo.}) \ ,$$

above but still consistent with the world average value of $\alpha_{\rm S}(M_{\rm Z^0}) = 0.1182 \pm 0.0027$ [28]. It has been observed previously in comparisons of distributions of event shape observables

with NLO QCD predictions with $x_\mu = 1$ that fitted values of $\alpha_S(M_{Z^0})$ tend to be large, see e.g. [29].

Combining only the fit results from $\langle 1-T \rangle$, $\langle C \rangle$, $\langle B_T \rangle$, $\langle B_W \rangle$, $\langle y_{23} \rangle$ and $\langle M_H^2 \rangle$ yields a value of

$$\alpha_S(M_{Z^0}) = 0.1239 \pm 0.0004(\text{stat.}) \pm 0.0008(\text{exp.}) \pm 0.0009(\text{had.}) \pm 0.0059(\text{theo.}) \; .$$

The slightly smaller error of α_S reflects the fact that the lower order moments are less sensitive to the multijet region of the event shape distributions. This leads to a smaller systematic uncertainty.

6 Summary

In this note we present preliminary measurements of the strong coupling constant from moments of event shape distributions at centre-of-mass energies between 14 and 44 GeV using data of the JADE experiment. The predictions of the PYTHIA, HERWIG and ARIADNE Monte Carlo models tuned by OPAL to LEP 1 data are found to be in reasonable agreement with the measured moments.

From a fit of $\mathcal{O}(\alpha_S^2)$ predictions to selected event shape moments corrected for experimental and hadronization effects we have determined the strong coupling constant to be $\alpha_S(M_{Z^0}) = 0.1286 \pm 0.0072$ (total error). The higher moments, in particular of the Thrust, C-Parameter and B_T event shape, lead to systematically enlarged value of α_S.

References

[1] B. Naroska: Phys. Rep. **148** (1987) 67

[2] JADE Coll., P.A. Movilla Fernández, O. Biebel, S. Bethke, S. Kluth, P. Pfeifenschneider et al.: Eur. Phys. J. C **1** (1998) 461

[3] JADE and OPAL Coll., P. Pfeifenschneider et al.: Eur. Phys. J. C **17** (2000) 19

[4] P.A. Movilla Fernández: In: ICHEP 2002: Parallel Sessions, S. Bentvelsen, P. de Jong, J. Koch, E. Laenen (eds.), 361. North-Holland, 2003

[5] S. Brandt, Ch. Peyrou, R. Sosnowski, A. Wroblewski: Phys. Lett. **12** (1964) 57

[6] E. Fahri: Phys. Rev. Lett. **39** (1977) 1587

[7] R.K. Ellis, D.A. Ross, A.E. Terrano: Nucl. Phys. B **178** (1981) 421

[8] T. Chandramohan, L. Clavelli: Nucl. Phys. B **184** (1981) 365

[9] L. Clavelli, D. Wyler: Phys. Lett. B **103** (1981) 383

[10] S. Catani, G. Turnock, B.R. Webber: Phys. Lett. B **295** (1992) 269

[11] S. Catani et al.: Phys. Lett. B **269** (1991) 432

[12] S. Catani, M.H. Seymour: Phys. Lett. B **378** (1996) 287

[13] R.K. Ellis, W.J. Stirling, B.R. Webber: QCD and Collider Physics. Vol. 8 of Cambridge Monographs on Particle Physics, Nuclear Physics and Cosmology, Cambridge University Press (1996)

[14] P.A. Movilla Fernández: Ph.D. thesis, RWTH Aachen, 2003, PITHA 03/01

[15] T. Sjöstrand: Comput. Phys. Commun. **82** (1994) 74

[16] G. Marchesini et al.: Comput. Phys. Commun. **67** (1992) 465

[17] G. Corcella et al.: J. High Energy Phys. **01** (2001) 010

[18] E. Elsen: *Detector Monte Carlos*, JADE Computer Note 54.

[19] E. Elsen: *Multihadronerzeugung in* e^+e^- *Vernichtung bei PETRA-Energien und Vergleich mit Aussagen der Quantenchromodynamik*, PhD thesis, Universität Hamburg, 1981.

[20] C. Bowdery and J. Olsen: *The JADE SUPERVISOR Program*, JADE Computer Note 73.

[21] L. Lönnblad: Comput. Phys. Commun. **71** (1992) 15

[22] R. Kuhn, F. Krauss, B. Ivanyi, G. Soff: Comput. Phys. Commun. **134** (2001) 223

[23] JADE Coll., W. Bartel et al.: Phys. Lett. B **88** (1979) 171

[24] JADE Coll., W. Bartel et al.: Phys. Lett. B **129** (1983) 145

[25] JADE Coll., S. Bethke et al.: Phys. Lett. B **213** (1988) 235

[26] Particle Data Group, S. Eidelman et al.: Phys. Lett. B **592** (2004) 1

[27] The LEP Experiments (ALEPH, DELPHI, L3 and OPAL) and the LEP QCD Working Group: paper in preparation

[28] S. Bethke: MPP-2004-88, hep-ex/0407021 (2004)

[29] OPAL Coll., P.D. Acton et al.: Z. Phys. C **59** (1993) 1

Figures

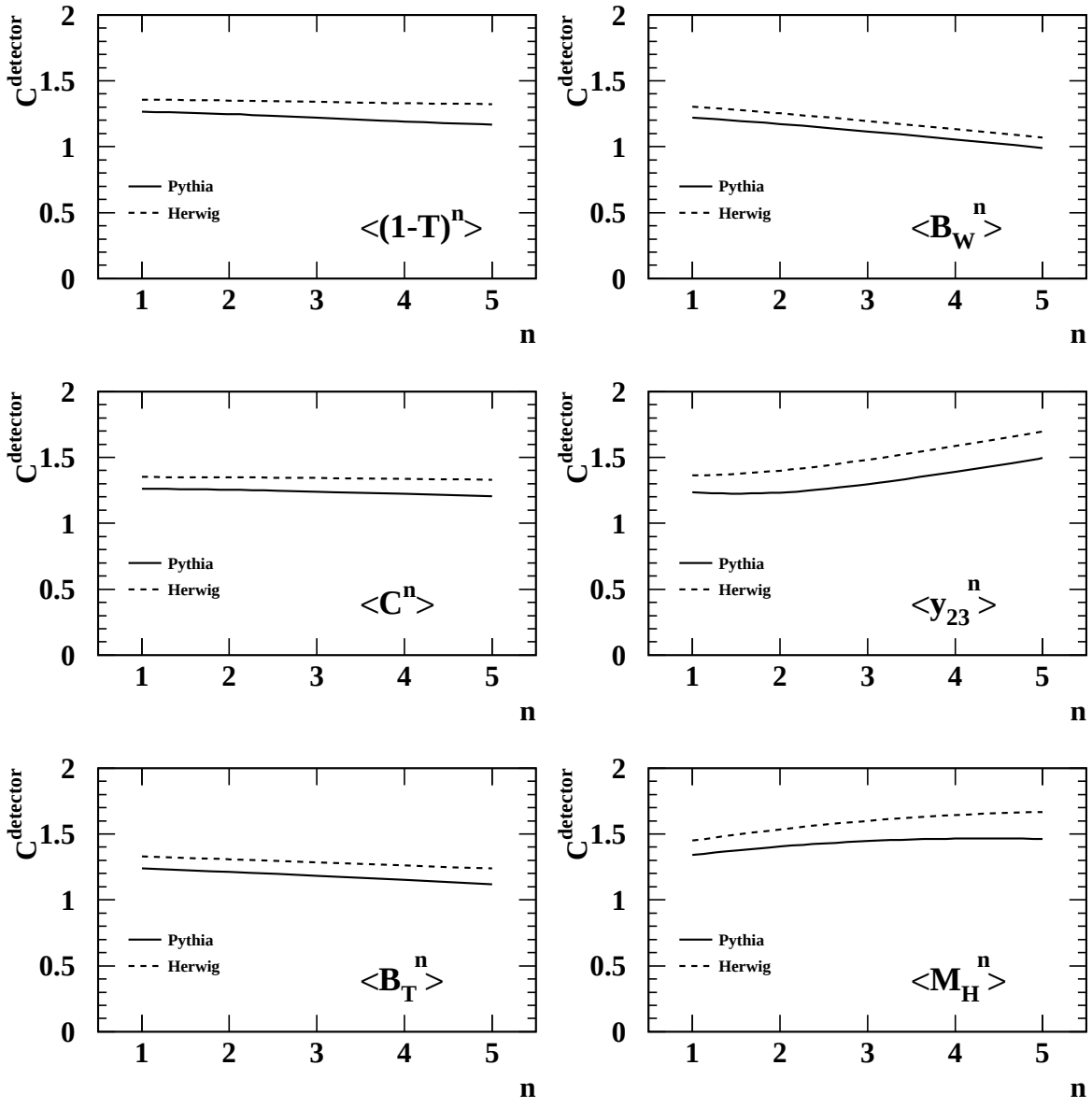

Figure 1: The figures show the detector corrections at $\sqrt{s} = 14$ GeV as calculated using PYTHIA and HERWIG.

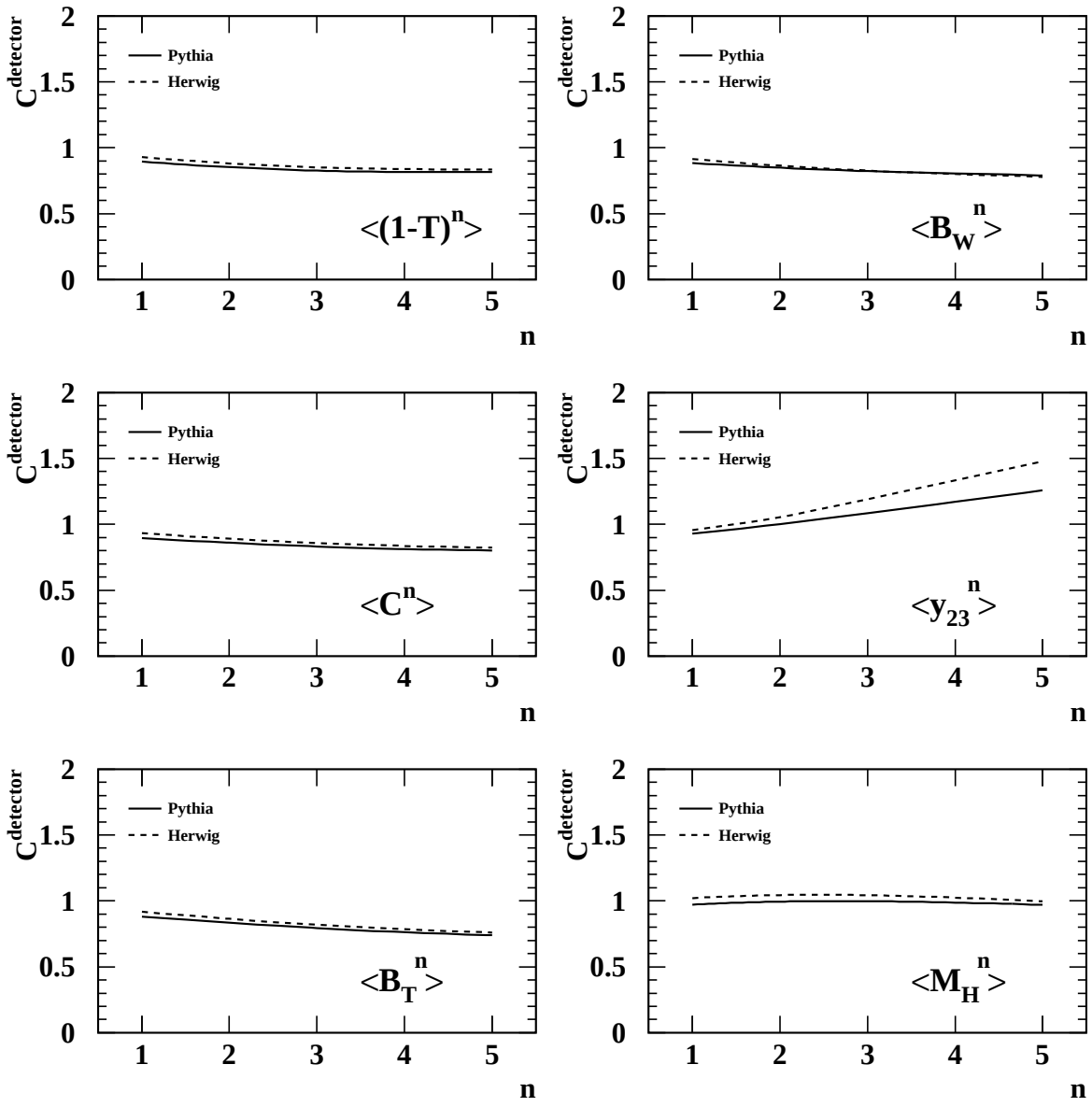

Figure 2: Same as figure 1 for $\sqrt{s} = 35$ GeV

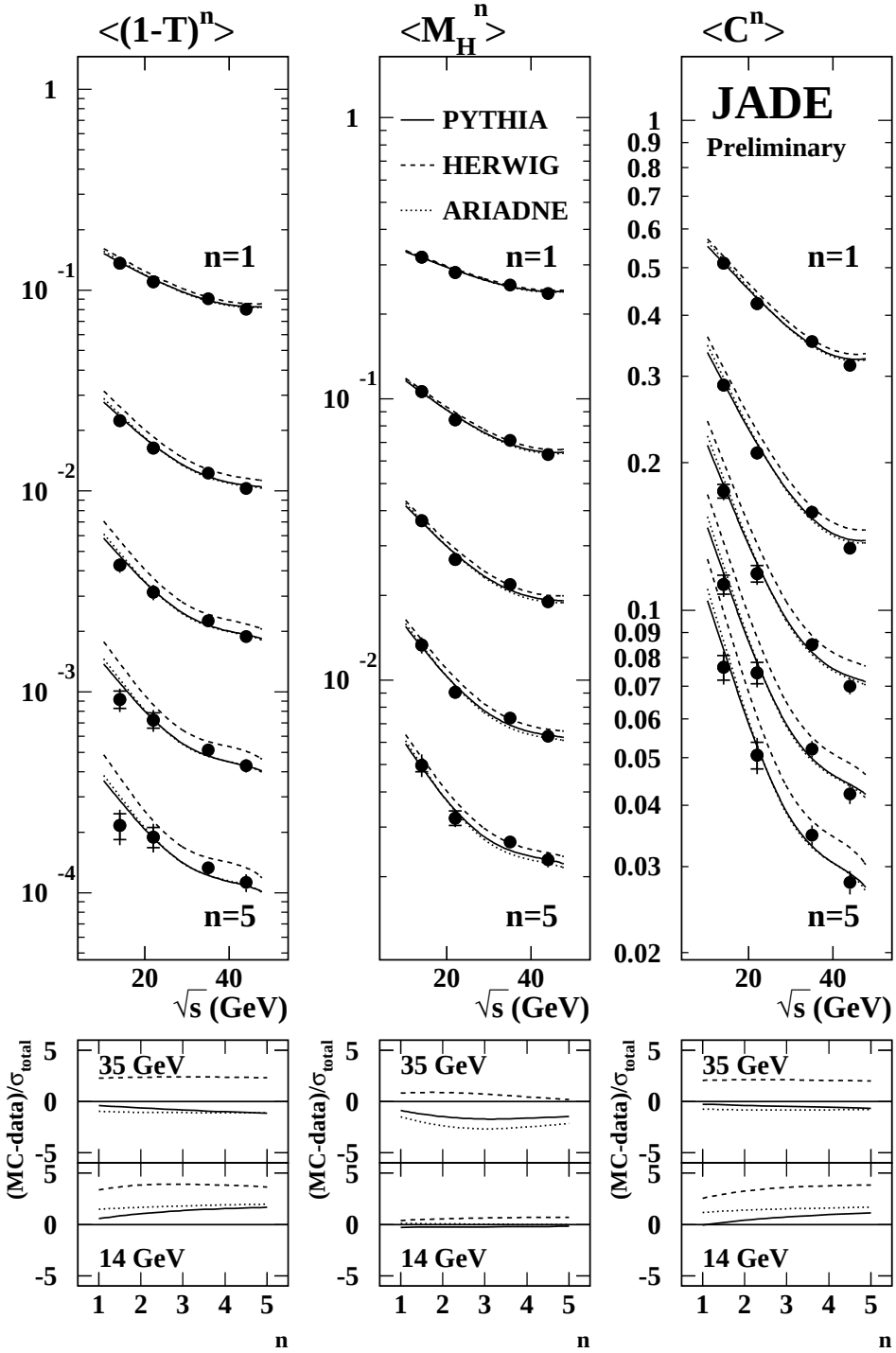

Figure 3: The figures show the first five moments of $1-T$, M_{H} and C at hadron level compared with predictions based on PYTHIA, HERWIG and ARIADNE Monte Carlo events. The errors shown include all statistical and experimental uncertainties. The lower panels show the differences between data and Monte Carlo at $\sqrt{s} = 14$ and 35 GeV, divided by the quadratic sum of the statistical and experimental error.

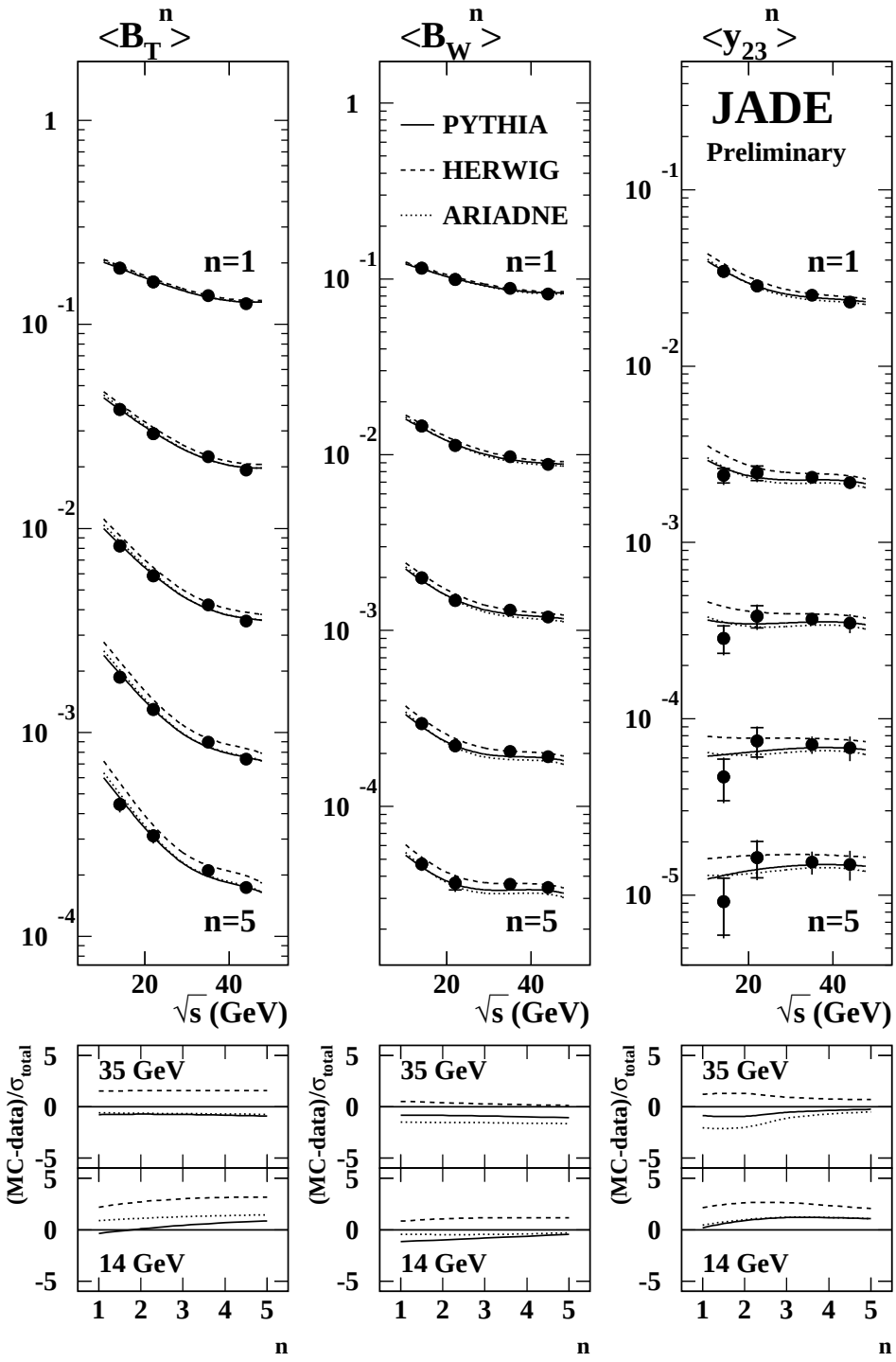

Figure 4: Same as figure 3 for B_{T}, B_{W} and y_{23}.

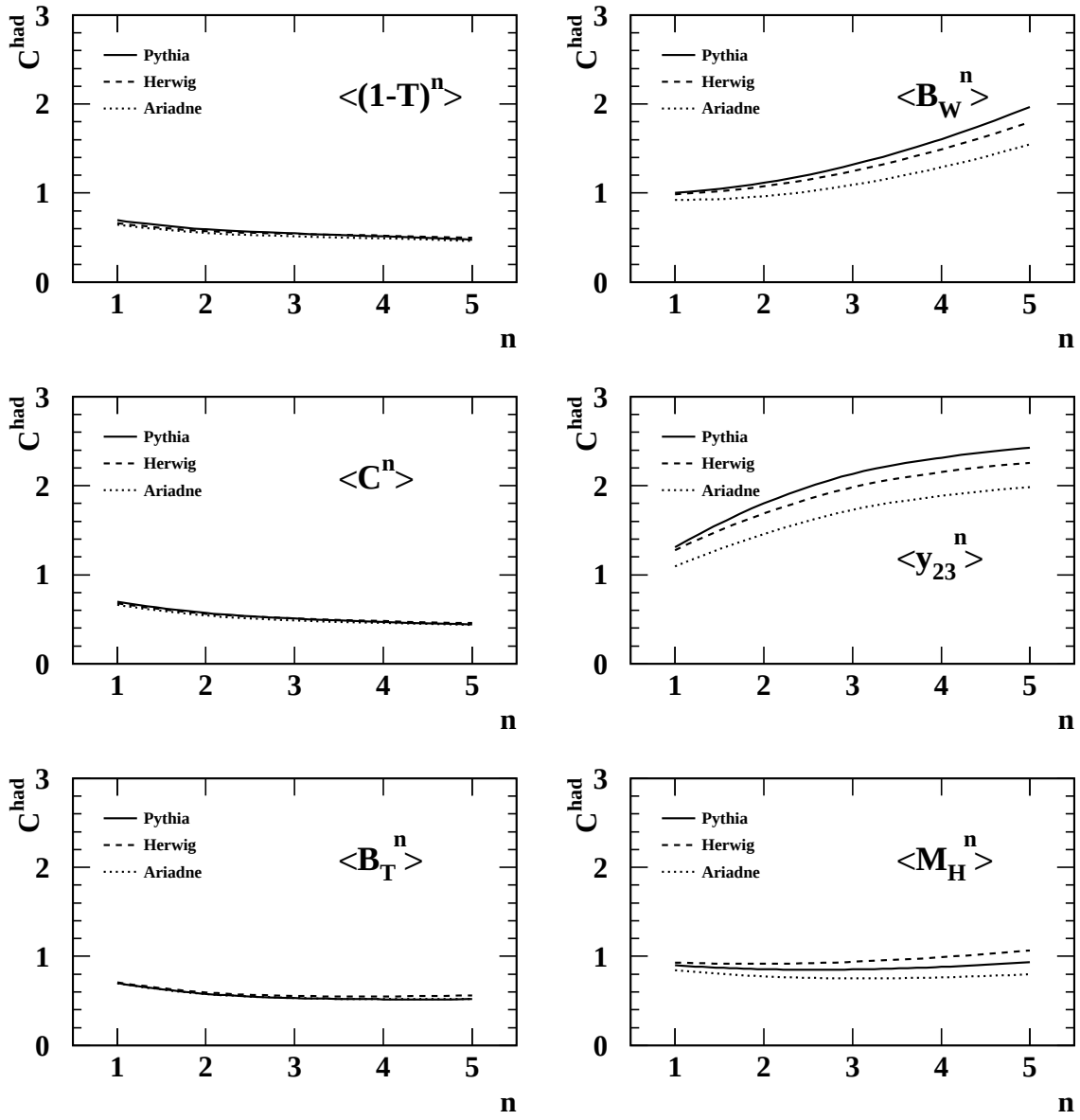

Figure 5: The figures show the hadronization corrections at $\sqrt{s} = 14$ GeV as calculated using PYTHIA, HERWIG and ARIADNE.

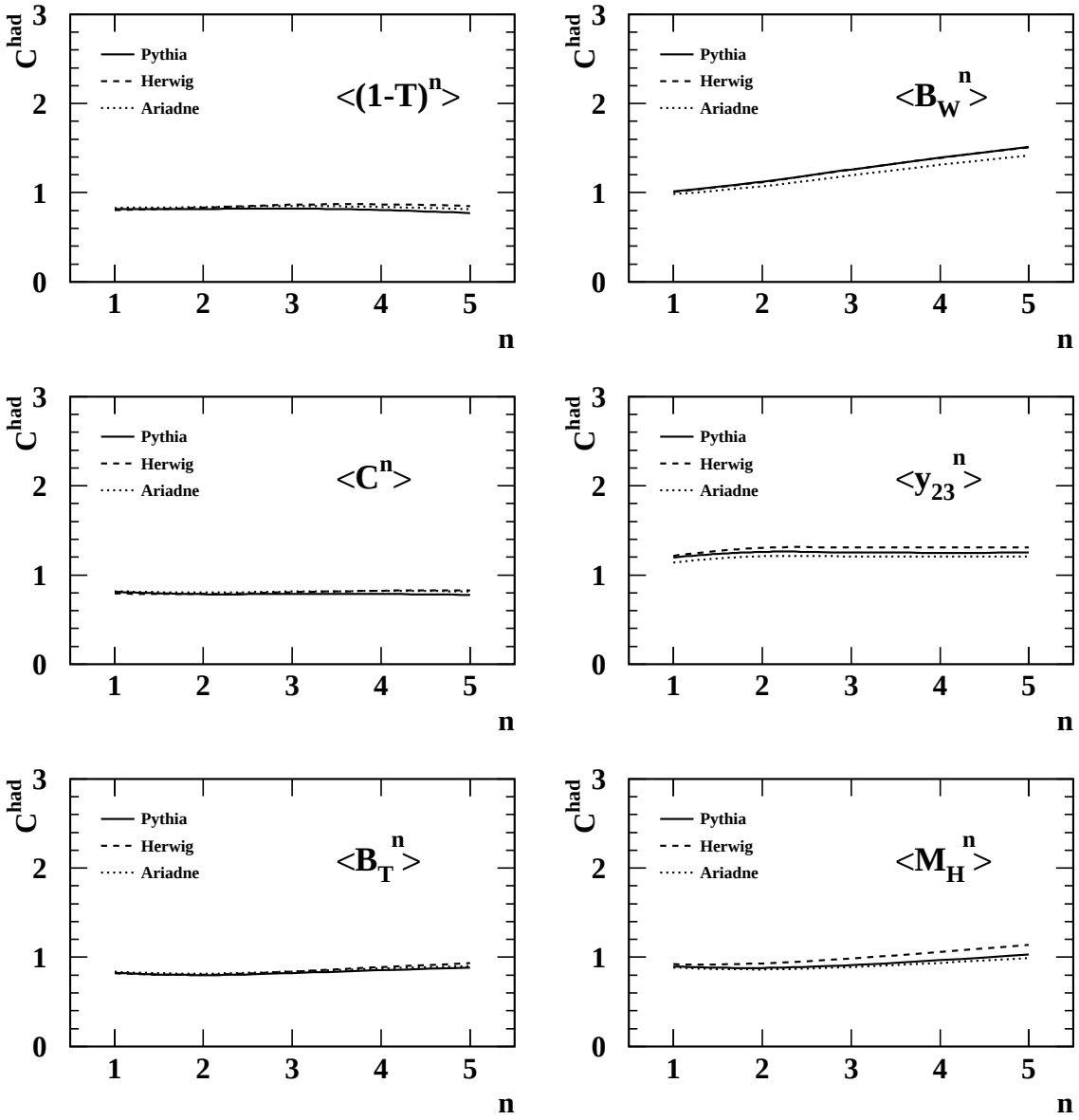

Figure 6: Same as fig. 5 for $\sqrt{s} = 35$ GeV.

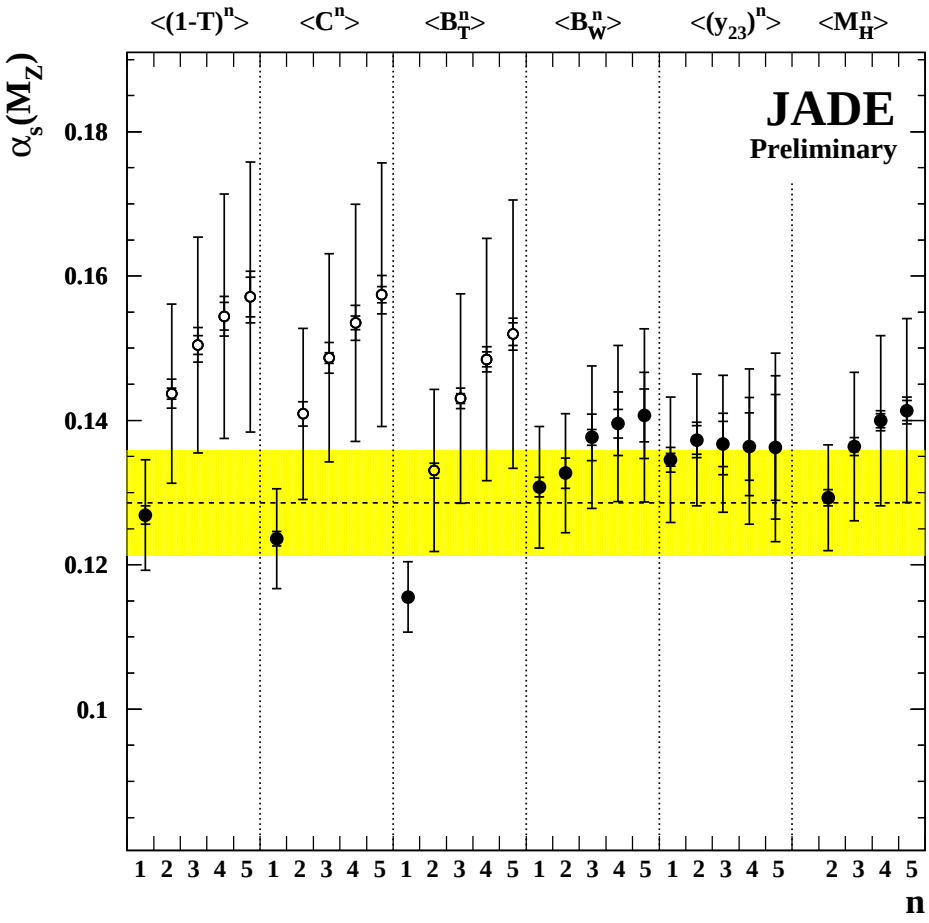

Figure 7: Measurements of $\alpha_S(M_{Z^0})$ using fits to moments of six event shape observables. The inner error bars represent statistical errors, the middle error bars include experimental errors and the outer error bars show the total errors. The dotted line indicates the weighted average described in the text; only the measurements indicated by solid symbols were used for this purpose.

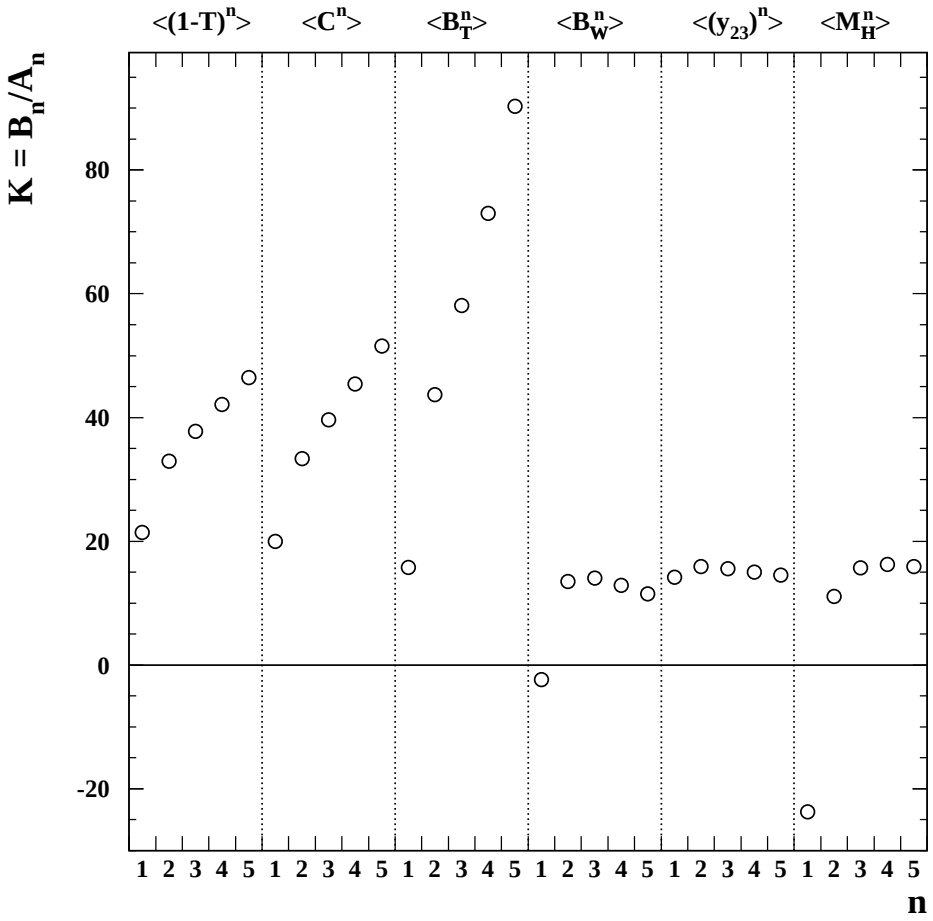

Figure 8: The ratio $K = \mathcal{B}_n/\mathcal{A}_n$ of NLO and LO coefficients for the six observables.